Radiation Physics and Chemistry 224 (2024) 112103

Contents lists available at ScienceDirect

Radiation Physics and Chemistry

journal homepage: www.elsevier.com/locate/radphyschem

Computed tomography imaging analysis of a fused filament fabrication (FFF) 3D printed neck-thyroid phantom for multidisciplinary purposes

D. Villani [a,b,*], M. Savi [a,c], O. Rodrigues Jr. [a], M.P.A. Potiens [a], L.L. Campos [a]

[a] *Instituto de Pesquisas Energéticas e Nucleares – IPEN/USP, Prof. Lineu Prestes Avenue 2242, São Paulo, Brazil*
[b] *Photo Injector Test Facility – PITZ, Deutsches Elektronen-Synchrotron DESY. Platanenallee 6, 15738, Zeuthen, Germany*
[c] *Instituto Federal de Educação, Ciência e Tecnologia de Santa Catarina – IFSC, Mauro Ramos Avenue 950, Florianópolis, Brazil*

ARTICLE INFO

Handling Editor: Dr. Chris Chantler

Keywords:
3D printing
FFF
Phantom design
Neck-thyroid

ABSTRACT

The application of the 3D printing technique for the development of low-cost phantoms is being investigated recently and requires a complex study of the interaction of printed materials with different types and qualities of radiation, as well as the characterization of printing filaments to correctly simulate human tissue attenuation. This study aims to present the Computed Tomography (CT) Imaging analysis of a fused filament fabrication (FFF) 3D printed anthropomorphic neck-thyroid phantom. The commercial phantom ATOM MAX 711 from CIRS was used as anatomy of reference for the 3D modeling base of the neck-thyroid phantom. Commercially available PLA and ABS XCT-A validated at IPEN were used in the 3D printing process in order to simulate soft and bone tissues respectively. The printing process was done using the RAISE3D PRO 2 FFF printer from IPEN. The imaging study of the phantom was performed through the analysis of images from a CT acquisition, comparing the Hounsfield Units (HU) numbers of the tissues between both CIRS and 3D printed phantoms. The developed phantom is a feasible alternative and presents some desirable characteristics for applications in radiation protection, measurements of radioisotopes incorporated in the thyroid (both contamination counters and nuclear medicine detectors) and training of techniques of acquisition of images with X rays.

1. Introduction

Since its conceptualization in the 1980s, three-dimensional (3D) printing techniques have been developed, matured, and used in various applications by many researchers and industrial companies worldwide. Nowadays it is revolutionizing manufacturing and many other areas of industry with new processes and materials with the potential to produce reproducible and sophisticated phantoms (Wang et al., 2017; Filippou and Tsoumpas, 2018).

The use of 3D printers and filaments commonly found commercially for the development of phantoms is being investigated and research is being carried out into some applications, including: quality control devices (Arconada-Alvarez et al., 2017; Odgen, Morabito and Depew, 2019); TC imaging (Hamedani et al., 2018); clinical electrons and photons dosimetry (Diamantopoulos et al., 2018; Pereira et al., 2021, 2022); developments of physical and anthropomorphic mammography simulators based on patient specific CT data; mathematical phantoms used for development and optimization of new breast imaging techniques; new realistic test models for X-ray breast dosimetry; and applied in image reconstruction and enhancement algorithms (Feradov et al., 2019; Daskalov et al., 2019; Esposito et al., 2019).

The application of this technique for the development of low-cost phantoms requires complex studies on interaction of printed materials with different types and qualities of radiation, as well as the characterization of printing configurations. By controlling these factors, it is possible to set methods that can correctly simulate human tissue within a printed phantom.

The Energy and Nuclear Research Institute (IPEN) from the University of São Paulo (USP) has experience in the field of development of 3D printed phantoms. Under the FAPESP project Nº 2017/50332-0 – Institutional Development Plans for Research from the State Research Institutes in the State of São Paulo, the Radiation Metrology Center has acquired state-of-the-art fused filament fabrication (FFF) RAISE 3D PRO2 3D printer. Previous research has already been carried out using this equipment, specially on filaments attenuation characterization (Villani et al., 2020; Savi et al., 2020; Savi et al., 2021).

Thus, this study aims to provide a comprehensive Computed Tomography (CT) imaging analysis of an FFF 3D printed anthropomorphic

* Corresponding author. Instituto de Pesquisas Energéticas e Nucleares – IPEN/USP, Prof. Lineu Prestes Avenue 2242, São Paulo, Brazil.
E-mail address: dvillani@ipen.br (D. Villani).

https://doi.org/10.1016/j.radphyschem.2024.112103
Received 1 March 2024; Received in revised form 22 July 2024; Accepted 30 July 2024
Available online 31 July 2024

Fig. 1. Atom MAX 711 phantom used as reference for this study https://www.cirsinc.com/products/diagnostic-ct/atom-max-dental-diagnostic-head-phantom/.

neck-thyroid phantom, incorporating Epoxy resin for the thyroid inner content. Utilizing the anatomy of the commercial phantom ATOM MAX 711 from CIRS, our aim was to develop a cost-effective alternative that offers comparable Hounsfield Units and anatomical fidelity for CT imaging analysis. The presented neck-thyroid phantom not only serves as a replacement for the CIRS 711 Atom Max phantom, but also has potential for diverse research applications in various disciplines.

2. Experimental

2.1. Design and construction of the 3D printed phantom

The 3D printing.STL files used in this work were obtained with an anatomical reference for modeling: the head and neck ATOM 711 phantom from CIRS (Fig. 1). This anatomy chosen complies with the dimensions of a standard man according to international formalisms (Goldstone, 1989; IAEA, 2007). The ATOM 711 phantom is primarily designed for determining optimal settings for an X-ray imaging system, commissioning new equipment, monitoring system performance, and procedural training. The manufacturer does not specify the composition of its construction materials; only describes that it is made from epoxy resins that mimic the X-ray attenuation properties of human tissue for CT and therapy energy ranges (50keV-25MeV) (ATOMMax® CIRS 711-H Specification sheet, 2024).

From a computed tomography (CT) of this phantom, made available by the collection of the Federal Institute of Education, Science and Technology of Santa Catarina – IFSC, the three-dimensional model was obtained to be used for 3D printing using the '3D Slicer' segmentation

Table 1
Imaging protocol used in the study.

Tension (kVp)	Current (mA)	Slice thickness (mm)	Time (s)	Current-time product (mAs)
120	50	2.0	5.2	260

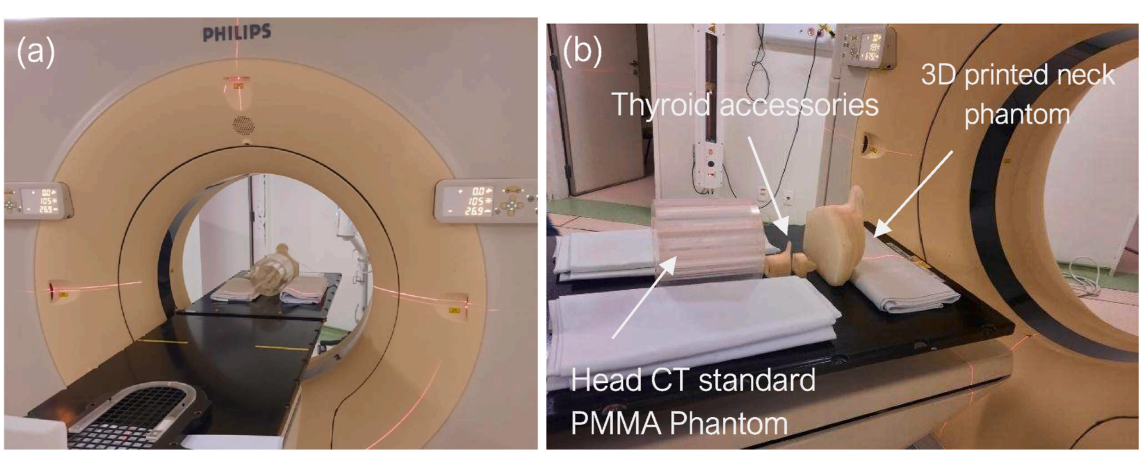

Fig. 2. Phillips Brilliance Big Bore Radiology CT scanner and phantoms used in the study. (a) Phantoms positioned on the CT scanner couch (b) Details on the phantoms to be imaged.

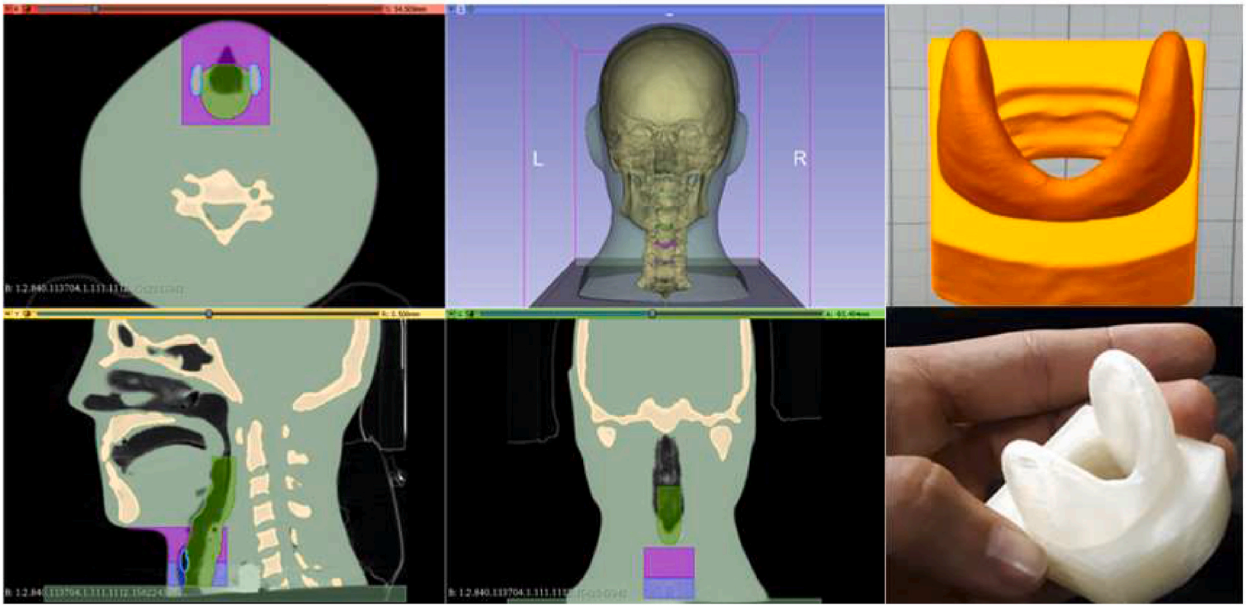

Fig. 3. Contouring of the 3D model of the phantom using 3Dslicer software. On detail the thyroid accessory.

software. This software works similar to a radiotherapy planning system, and the structures were countering slice by slice resulting the final 3D model.

2.2. 3D printing configuration

The attenuation behavior of a variety of 3D printed filaments, as well as the new developed ABS XCT-A filament were previously studied. The complete study regarding the attenuation properties of the materials as well as comparison with theoretical data can be found in Villani et al. (2020); Savi et al. (2021); Savi et al. (2022). These previous studies enabled our choice of materials and printing set up.

For PLA the main printing configurations used were: 2 external continuous lines and 100% rectilinear filling with orientation +45°/-45°. For ABS XCT-A was also configured 2 external continuous lines (cortical bone), and 45% infill (trabecular bone). For operational reasons (supplying inputs into the printer, monitoring operation and electricity), the phantom was segmented into slabs to be printed. Each of the segments was about 2.0 cm high and each piece has an estimated average printing time of 22 h.

2.3. Neck-thyroid accessory

The thyroid was designed as a removable neck attachment, as an accessory. This accessory can be used as radioactive source immobilized with epoxy resin for nuclear medicine imaging and quality assurance. Some dosimetric and radiation protection applications also require the use of phantom-sources for equipment calibration. In the case of internal thyroid contamination or acquisition tests in nuclear medicine, the radioactive source object may be the thyroid itself. In this sense, it is necessary to enable a technique that keeps the radioactive material only in the region of interest without the occurrence of leaks or external contamination. The Center for Radiation Technology (CTR-IPEN) develops sealed reference sources immobilizing radioactive isotopes in epoxy resin (Cerqueira and Maia, 2014) and this technique is suitable for immobilizing sources within 3D printed parts. To this aim, the thyroid was printed with no 3D printing infill and later filled with epoxy resin for analysis.

2.4. CT imaging acquisition and analysis

The analysis of images from a computed tomography (CT) acquisition can be part of the usability validation of the phantom. This method involves a structured comparison of Hounsfield Unit numbers (HU, also referred to as CT numbers) obtained from both the 3D printed phantom and the ATOM CIRS 711 phantom. The Hounsfield scale is related to obtaining X-ray images and transforms the different shades of gray, acquired in X-ray imaging, into numerical values inherent to the attenuation properties of materials.

A preliminary procedure, before any study on a given piece of equipment, is the verification of its operating conditions within the regulated requirements for its use. This evaluation is normally performed as part of the imaging quality control tests of the equipment, defined and specified by regulation (ANVISA, 2005; IAEA, 2007).

The tomographic images were acquired with a Phillips Brilliance Big Bore Radiology CT scanner from the Cancer Institute of the State of São Paulo – ICESP (see Fig. 2). For preliminary quality control, a standard cylindrical PMMA phantom (16 cm in diameter, 15.5 cm in depth) from LCI-IPEN was used to analyze the standard quality properties of the equipment, followed by the 3D printed neck phantom and the epoxy resin-filled thyroid accessory. Every element was imaged in the same acquisition with the protocol showed in Table 1.

Image analyzes was done using the measurement tools (ROIs and ruler) of the Weasis v3.7.0 software, and it was possible to perform:

- o Analysis of soft tissue construction with PLA;
- o Analysis of the construction of bone tissues with ABS XCT-A;
- o Analysis of the construction of the thyroid accessory with epoxy resin;
- o Analysis of the fit spacing of the printed pieces;
- o Analysis of artifacts in the image using the FFF technique.

The imaging analyses was done at correspondent slices between the two phantoms, one by one, but the results in this paper are presented at a chosen slice for better illustration.

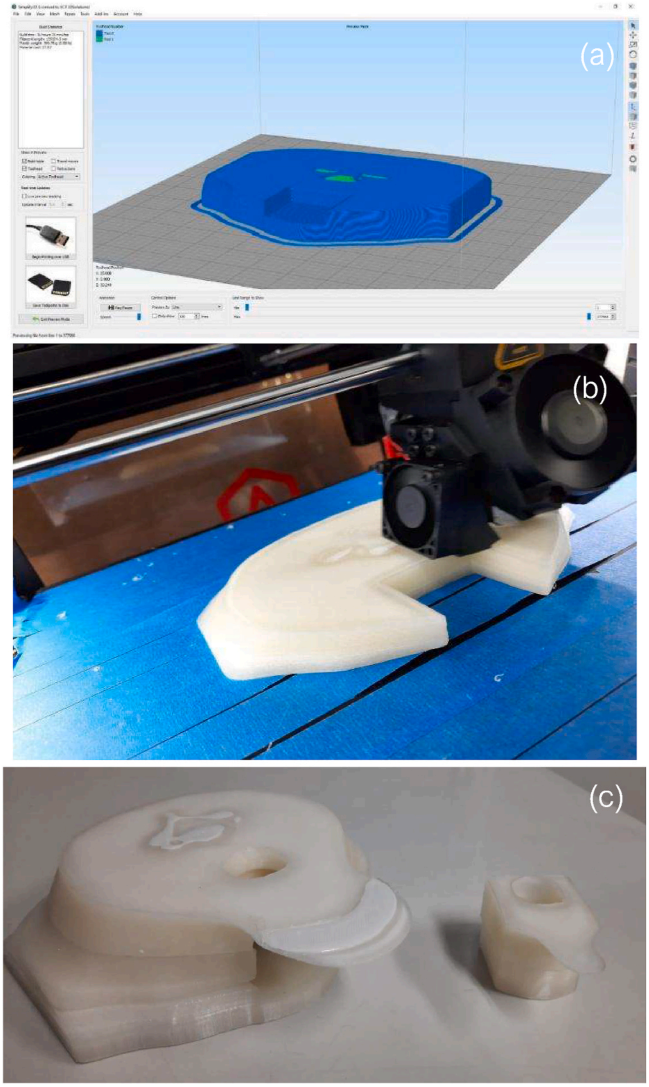

Figs. 4. 3D printing of the phantom. (a) '3D slicer' configuration of slab printing parameters (b) 3D printing of a slab (c) Final neck-thyroid phantom obtained.

3. Results

3.1. 3D construction of the anthropomorphic phantom

Using the 3DSlicer software and a CT scan from the CIRS 711 simulator, similar to a radiotherapy planning system, the structures were contoured slice by slice, resulting in the 3D model shown in Fig. 3. Then the thyroid accessory was drawn. To facilitate the printing logistics, the 3D design of the phantom was sectioned into 20 mm high slices.

3.2. Printing of the phantom

After conducting thorough our attenuation analyses (Villani et al., 2020; Savi et al., 2020; Savi et al., 2021), it was determined that the optimal 3D printing filaments for developing the phantom in this study are PLA for equivalence with PMMA/soft tissue, and XCT-A radiopaque ABS, validated at IPEN (Savi et al., 2022) for bone equivalence. The 3D phantom, with a height of 20 mm, was subsequently segmented into "slices" and configured for printing using Simplify3D software. Fig. 4 showcases an example of a generated print *.STL file and the fully printed neck-thyroid phantom. It is worth to mention that the printer utilized features two extruders, enabling the utilization of different materials within the same piece without necessitating additional hardware or software.

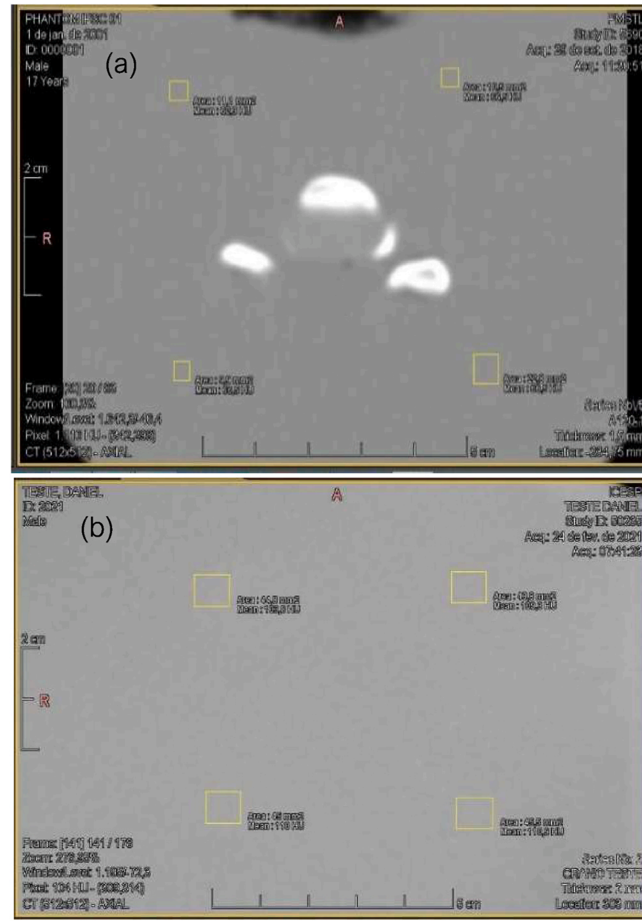

Fig. 5. (a) Investigation of CT numbers obtained from "soft tissues" of the CIRS 711. (b) Investigation of CT numbers obtained from "soft parts" of the 3D printed phantom.

Table 2
CT numbers resulting from analysis on CIRS 711 simulators and 3D printed for soft tissue simulation.

	CIRS 711		3D		R (3D/CIRS)[a]	
Upper ROIs	Right	Left	Right	Left	Right	Left
Soft Tissue (HU)	62.3	66.5	102.8	109.3	1.650	1.644
SD	3.2	2.5	8.4	6.0		
CV	5.1%	3.8%	8.2%	5.5%		
Lower ROIs	Right	Left	Right	Left	Right	Left
Soft Tissue (HU)	66.5	66.5	110.2	110.9	1.657	1.668
SD	3.4	3.4	4.7	5.7		
CV	5.1%	5.0%	4.3%	5.1%		

[a] R = the ratio between the HU values obtained from the printed and the reference phantom.

3.3. Preliminary imaging QA results

As expected, the Phillips Brilliance Big Bore Radiology CT scanner used for there measurements was in accordance with the requirements of the formalisms and previous quality control results.

3.4. Analysis of soft tissue construction with PLA

PLA was chosen as the material to be used in the 3D printing of parts

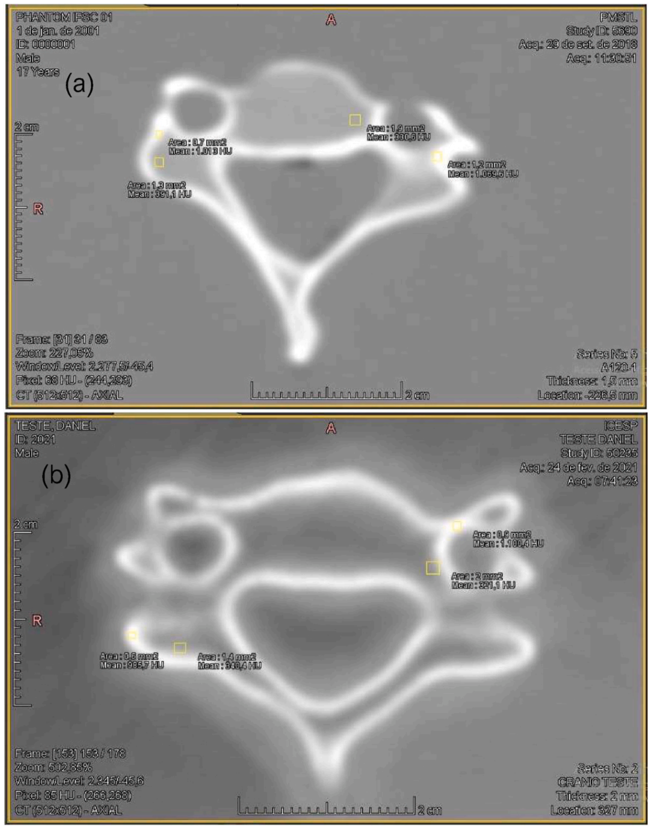

Fig. 6. (a) Investigation of CT numbers obtained from "bone tissues" of the CIRS 711 phantom. (b) Investigation of CT numbers obtained from "bone tissues" of the 3D printed phantom.

Table 3
CT numbers resulting from analysis on CIRS 711 and 3D printed phantoms for bone tissue representation.

	CIRS 711		3D		R (3D/CIRS)[a]	
Upper ROIs	Right	Left	Right	Left	Right	Left
Cortical Bones (HU)	1013	1069.6	985.7	1100.4	0.973	1.029
SD	63	140.1	221.3	54.8		
CV	6.2 %	13.1%	22.5 %	5.0 %		
Lower ROIs	Right	Left	Right	Left	Right	Left
Trabecular Bones (HU)	391.1	330.6	340.4	321.1	0.870	0.971
SD	33.3	5.4	125.5	236.0		
CV	8.5 %	1.6 %	36.9 %	73.5 %		

[a] R = the ratio between the HU values obtained from the printed and the reference phantom.

that simulate "soft tissue" due to its attenuation close to PMMA studied in previous analyzes (Villani et al., 2020). Fig. 5 and Table 2 show the results of CT numbers obtained using Weasis v3.7.0 software for the CIRS 711 phantom and the PLA printed areas of the 3D printed phantom, with respectively standard deviation (SD) and Coefficient of Variation (CV) values.

Analyzing these results one can observe that the construction of the CIRS soft tissue has a CT number of 65.5 ± 1.8 HU, with coefficients of variation between 3.8% and 5.1%. Little information about the materials used in the construction of this phantom is given by the manufacturer besides that it is made of epoxy resin (ATOMMax® CIRS 711-H Specification sheet, 2024), so these HU values were used as reference.

The PLA soft tissue construction has CT numbers of 108.3 ± 3.2 HU, a value 65.5 ± 0.9 % higher than in the CIRS phantom; and with higher coefficients of variation, ranging from 4.3 % to 8.2 %. The higher coefficients of variation for this material are justified by the intrinsic characteristics of the FFF printing technique and more details on them will be given in sections 3.8 and 3.9.

3.5. Analysis of the construction of bone tissues with ABS XCT-A

ABS XCT-A developed by Savi et al. (2022) and validated at IPEN was chosen as the material to be used in the 3D printing the bone tissues of the phantom. Fig. 6 and Table 3 show the results of CT numbers obtained for both phantoms.

Upon analysis of these images, one can observe that the CIRS bone tissue construction exhibits varying CT numbers of 1041 ± 28 HU for cortical bones with coefficients of variation ranging between 6.2% and 13.1%, and 360.9 ± 3.0 HU for trabecular bones with coefficients of variation ranging between 1.6 % and 8.5 %.

In comparison, the construction of bone tissue with ABS XCT-A yields CT numbers ranging from 1043 ± 57 HU for cortical bones with coefficients of variation between 5.0% and 22.5%, and 330.8 ± 9.6 HU for trabecular bones with coefficients of variation between 36.9% and 73.5%. As expected, bone tissue exhibits extreme irregularity and encompasses a broad spectrum of attenuation properties.

These findings demonstrate a concordance of approximately 96.1% between the reference and 3D printed simulators, further supporting the ABS XCT-A attenuation studies conducted by Savi et al. (2022). The elevated coefficients of variation (CV) values for both phantoms highlight the variability in bone tissue attenuation. However, it is observable that these values were notably higher in the 3D printed simulator, attributed to the intrinsic characteristics of the FFF printing technique. Adjusting infill percentages to exceed the 45% utilized in the printing of this phantom may mitigate this effect.

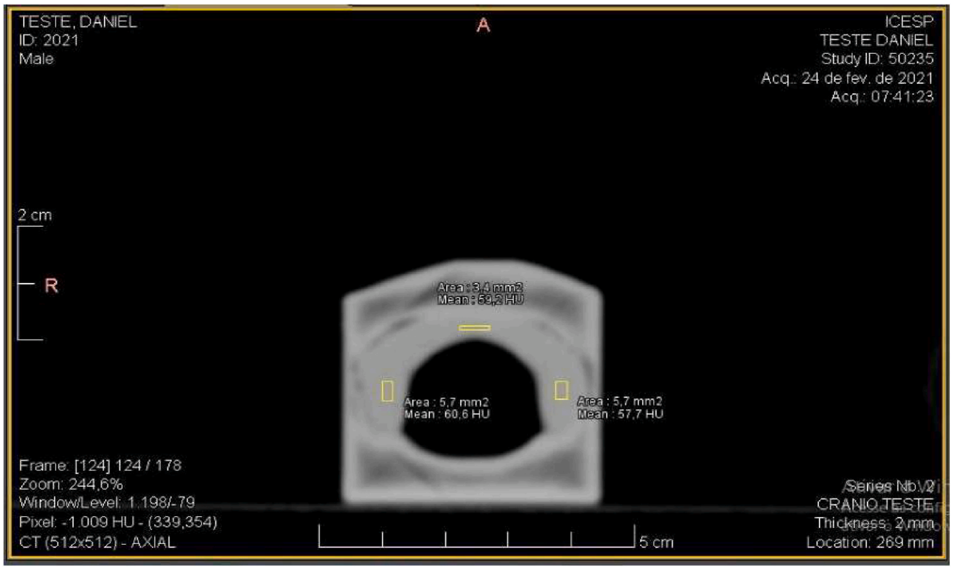

Fig. 7. Investigation of the CT numbers obtained for the epoxy resin incorporated into the 3D printed thyroid accessory.

Table 4
CT numbers resulting from analysis of the epoxy resin on the printed thyroid accesory

	Epoxy resin within the Thyroid			
Position	Left	Center	Right	Mean
Resin Value (HU)	60.6	59.2	57.7	59.2
SD	1.9	2.6	3.4	1.5
CV	3.1 %	4.4 %	5.8 %	2.5 %

3.6. *Analysis of the construction of the thyroid accessory with epoxy resin*

The construction of the thyroid accessory was carried out with printed PLA with the thyroid volume filled with epoxy resin afterwards in order to make it possible to immobilize radioactive sources for internal contamination and nuclear medicine imaging purposes in future studies. Fig. 7 and Table 4 show the results of CT numbers obtained for the epoxy resin inside the printed thyroid.

Analyzing the image, it can be seen that the epoxy resin incorporated into the thyroid accessory has average CT number values of 59.2 ± 1.5 HU, with coefficients of variation between 2.5 % and 5.8 %. These results show great homogeneity of the material inside the printed part. When we observe the CT number values presented in the soft tissue simulation in the CIRS 711 simulator (65.5 ± 0.9 HU, specified as epoxy resin by the manufacturer), the values measured in the accessory match $\sim$ 90.4 %.

Although the CT number values of the resin incorporated into the accessory are homogeneous, air bubbles of different sizes are observed

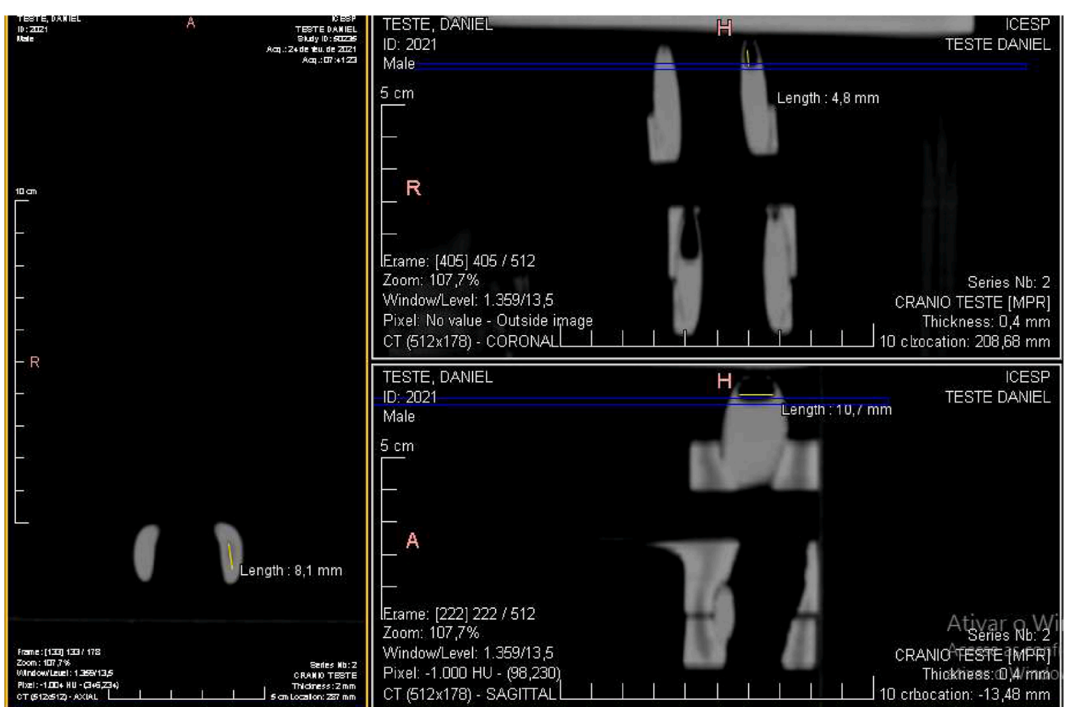

Fig. 8. Investigation of the dimensions of the air bubbles of the thyroid accessory.

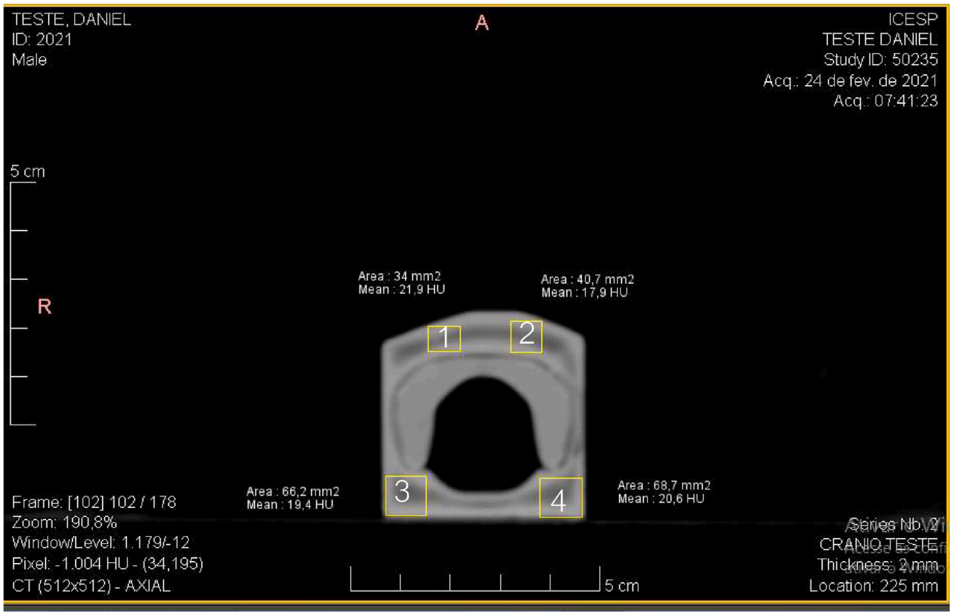

Fig. 9. Investigation of CT numbers obtained for PLA in the thyroid accessory.

Table 5
CT numbers resulting from analysis of the PLA printed on the thyroid accessory.

	PLA of the Thyroid accessory				
Position #	1	2	3	4	Mean
HU	21.9	17.9	19.4	20.6	20.0
SD	3.8	3.9	3.3	2.6	1.7
CV	17.4 %	21.8 %	17.0 %	12.6 %	8.6 %

inside the thyroid volume. Fig. 8 show the dimension analysis of the accessory's air bubble.

As also observed in the visual inspection, the epoxy resin incorporated in the accessory presented small air bubble of approximately ~5 x 8 × 11 mm^3. This fact indicates the need for and importance of high carefulness when manipulating the accessory, as the incorporated resin may contain radioactive material for specific applications.

An additional characteristic of the printed thyroid accessory is a change in CT number for PLA in regions peripheral to the thyroid. Fig. 9 and Table 5 show this data.

Upon closer examination of the image, a subtle increase in radiolucency is visible in the surrounding the thyroid geometry. This alteration contributes to a change in the average CT number of the printed PLA in comparison to soft tissue analysis, measuring 20.0 ± 1.7 HU. The coefficient of variation for these analyzed values ranged between 8.6% and 21.8%. This phenomenon can be attributed to the consistent print speed employed during FFF printing configuration.

In regions featuring details and borders, the printing speed may have influenced the deposition rate of PLA, thereby resulting in a reduction in CT number values. However, this observation does not detract from the usability of the piece, as these CT values effectively replicate the properties of superficial soft tissues in the body, such as skin and fat (Savi et al., 2020).

3.7. *Analysis of the fit spacing of the printed pieces*

In the printing methodology utilized to create this phantom, it was imperative to segment pieces approximately 2.0 cm in height and subsequently assemble them to form the final piece. Consequently, a notable characteristic emerged: the presence of interstices between these assembled pieces. Fig. 10 illustrates the findings of our investigation aimed at quantifying these spacings.

Upon analysis, it was determined that, on average, the pieces exhibit a spacing of 1.3 mm between them. However, larger gaps measuring 2.2 mm and 3.5 mm were observed in the posterior fitting of the thyroid accessory and the posterior neck, respectively. The latter value was attributed to a printing warp during the fabrication process.

It is worth documenting that a consequence of these small spacings between the pieces is that they can cause image "mismatches" between slices of the CT image. Fig. 11 exemplifies this phenomenon, causing slight discontinuities between images in subsequent cuts.

3.8. *Analysis of artifacts in the image using the FFF technique*

Upon analysis of the images obtained from the 3D printed phantom using the FFF technique, artifacts were observed stemming from inherent characteristics and operational challenges of the printing process. Among the notable artifacts, there was the presence of the print pattern, characterized by lines oriented at +45°/-45° angles. Additionally, the visualization of extrusion flaws was identified, manifesting as areas of increased radiolucency where insufficient material deposition occurred. Fig. 12 illustrates examples of both artifacts.

4. Discussions

The printing filaments utilized were evaluated for their radiation attenuation properties. It is worth to acknowledge that further investigations are necessary to ascertain their equivalence to human tissue in accordance with publication 44 of the International Commission on Radiation Units and Measurements (Goldstone, 1989). The formalism indicates that the validation of the tissue equivalence of materials involves evaluation of various parameters, including chemical composition, mass attenuation coefficient, mass stopping power, bulk density, electronic density, depth dose profile, and Hounsfield Units. Previous studies have provided the validation of PLA as a suitable soft tissue substitute for 3D printing of phantoms for radiotherapy applications (Pereira et al., 2021, 2022). While ABS XCT-A exhibits promising characteristics and its attenuation behavior has been benchmarked against theoretical data (Savi et al., 2022), a comprehensive understanding of its performance in mimicking human tissue properties requires additional validation.

Additionally, it's important to note that our imaging protocol

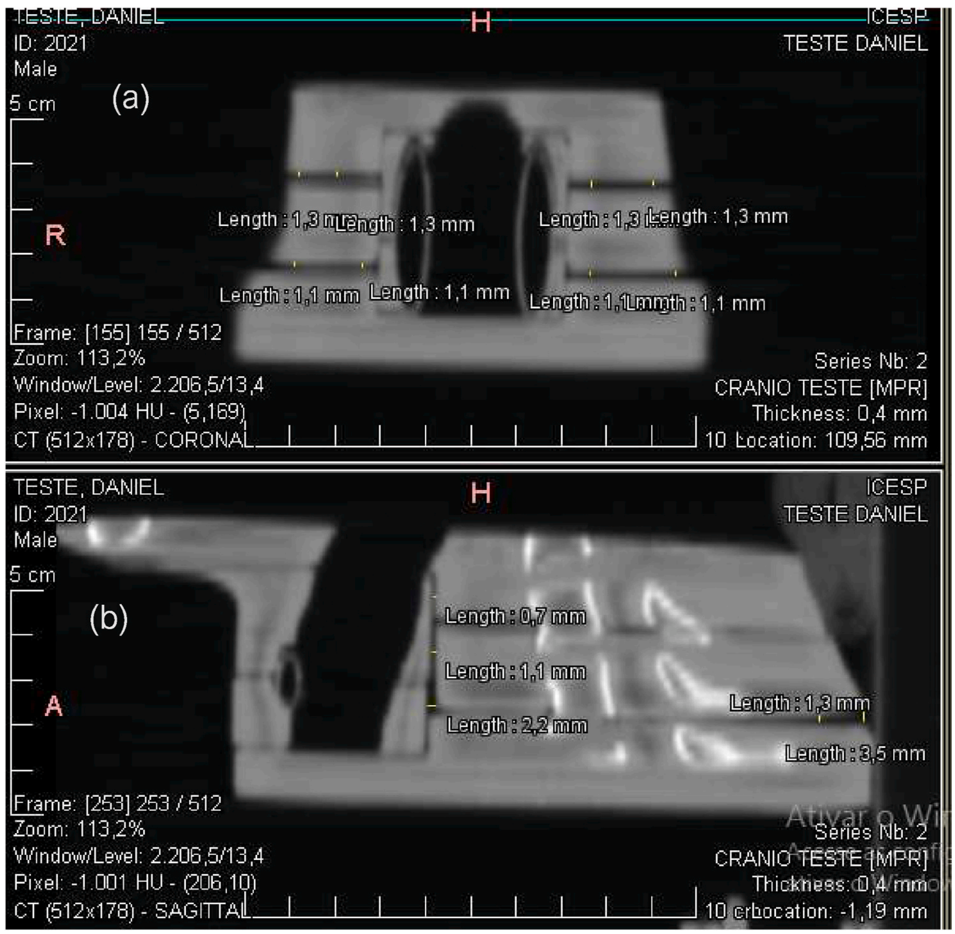

Fig. 10. Investigation of the fitting spacing between the simulator parts. (a) coronal section (b) sagittal section.

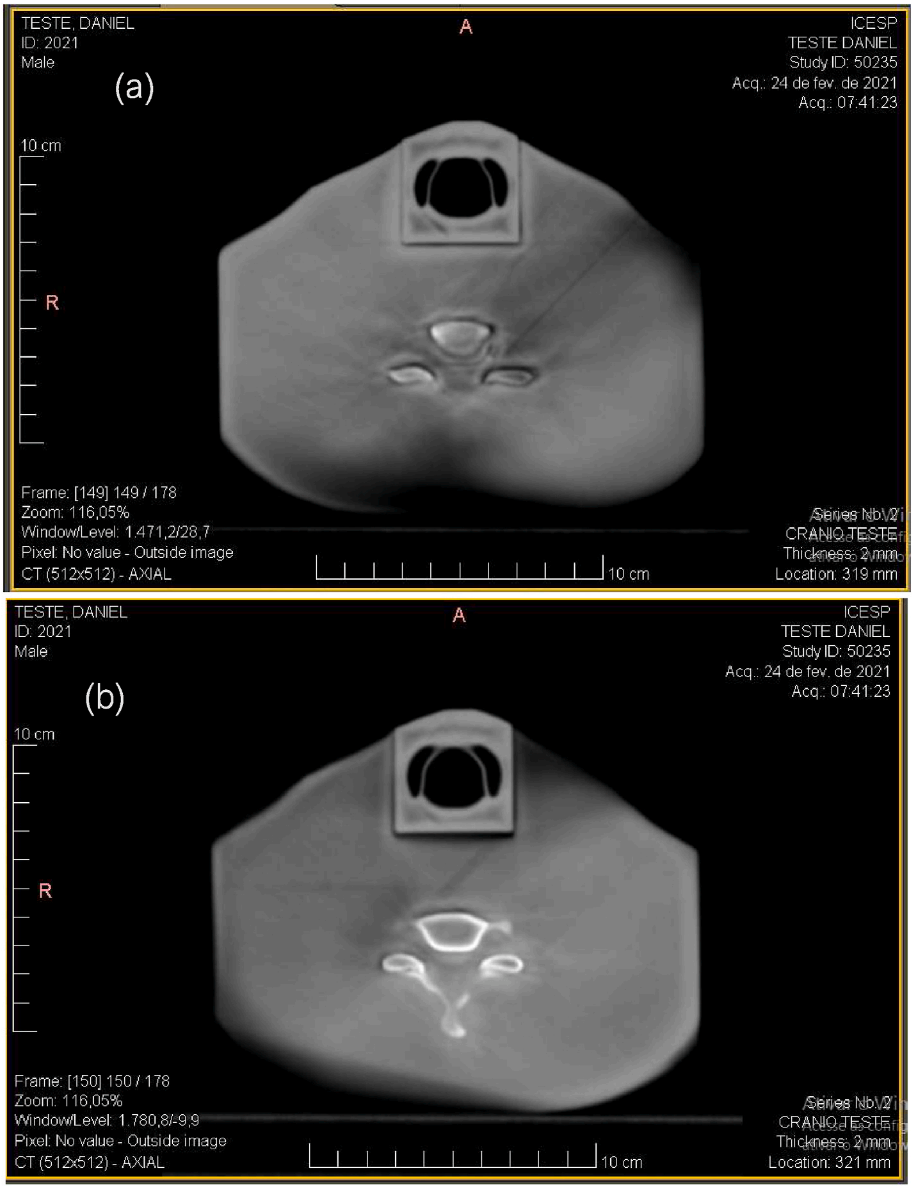

Fig. 11. Image extracted from Weasis v3.7.0 software exemplifying a consequence of the fitting spacing for the imaging of the 3D printed phantom (a) Slice location 319 mm (b) Slice location 321 mm.

involved a single acquisition to capture all images for analysis. While this approach offers efficiency, it introduces potential equipment calibration errors. These errors may be negligible when comparing results 1:1 using the CIRS ATOM MAX as a reference; and preliminary imaging quality measurements were done to ensure the quality of the results.

The analysis of CT numbers presented in this study comes with inherent limitations, primarily due to its simplification into 2D plans for analysis, thus not representing a comprehensive 3D measurement. While informative, this approach may overlook nuances present in the complete three-dimensional structure. Despite the limitations inherent to the presented data analysis, the 3D printed phantom developed in this study demonstrates promising results for its use in multidisciplinary applications.

It is also worth mentioning that CT reconstruction algorithms can also introduce imaging distortions, e.g. partial volume effects, as when a voxel contains multiple tissue types, resulting in signal averaging, loss of detail and anatomical differences between the object and the resulting image. These distortions can compromise diagnostic accuracy and require advanced correction techniques to minimize their impact (Koetzier et al., 2023), but were found negligible in the approach of data analysis chosen in this study.

5. Conclusions

The modeling methodology employed in this study shows a way for utilizing tomographic images of various objects, including patients, to facilitate the precise and customized fabrication of 3D phantoms. The analysis of CT images reveals promising outcomes, particularly in delineating the construction of soft tissues using PLA filaments, bone tissues utilizing ABS XCT-A, and the thyroid accessory employing epoxy resin. Additionally, it examines the fit spacing of printed components and addresses image artifacts arising from the FFF technique.

The resulting phantom stands as a viable option for studies in radiation applications, with favorable characteristics for applications in radiation protection, measurements of radioisotopes within the thyroid (both in contamination counters and nuclear medicine detectors), and

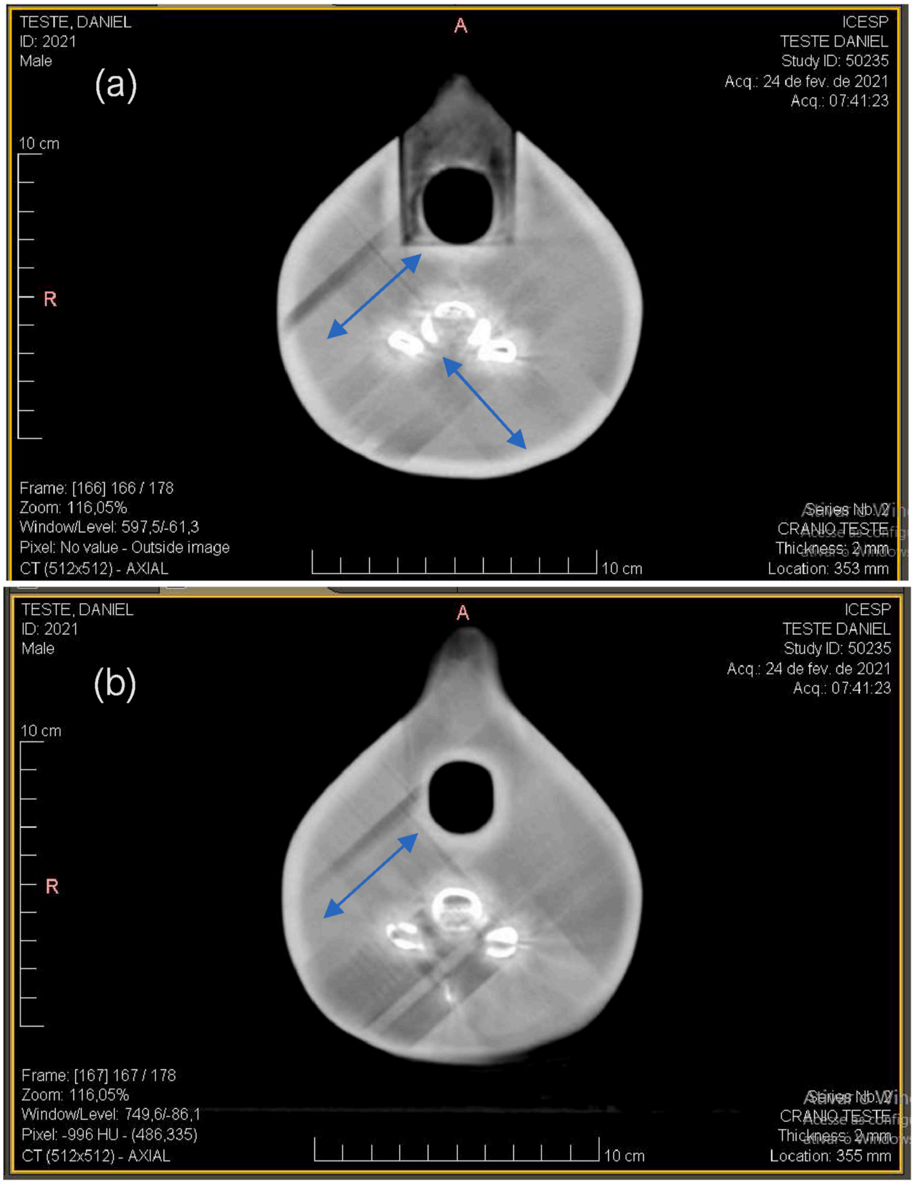

Fig. 12. Image exemplifying a consequence of the fitting spacing for the imaging of the phantom by computed tomography. (a) visualization of the impression lines (b) visualization of extrusion failure in the impression in the posterior part of the vertebra.

training in X-ray imaging acquisition techniques. Ongoing studies are underway to further evaluate the efficacy of this 3D phantom across some of these applications.

CRediT authorship contribution statement

D. Villani: Writing – original draft, Methodology, Investigation, Formal analysis, Data curation, Conceptualization. **M. Savi:** Writing – review & editing, Methodology, Investigation, Formal analysis. **O. Rodrigues:** Validation, Supervision, Project administration, Methodology, Formal analysis, Data curation. **M.P.A. Potiens:** Writing – review & editing, Data curation. **L.L. Campos:** Writing – review & editing, Formal analysis, Resources, Supervision.

Declaration of competing interest

The authors declare the following financial interests/personal relationships which may be considered as potential competing interests:

Leticia Lucente Campos reports financial support was provided by State of Sao Paulo Research Foundation. Daniel Villani reports financial support was provided by National Council for Scientific and Technological Development. If there are other authors, they declare that they have no known competing financial interests or personal relationships that could have appeared to influence the work reported in this paper.

Data availability

Data will be made available on request.

Acknowledgments

This work is dedicated to Dr. Campos, *in memoriam*, whose guidance, wisdom, and unwavering support have been invaluable. Your mentorship has not only shaped this paper but has also profoundly influenced my journey. I will forever carry your teachings and kindness in my heart (**D. Villani**). The authors would also would like to acknowledge the funding resources from FAPESP (process number 2017/50332-0), and from CNPq (process number 142098/2017-5) that supported this work.

References

Anvisa. Agência Nacional de Vigilância Sanitária, 2005. Radiodiagnóstico médico: segurança e desempenho de equipamentos. Editora Anvisa, Brasília, pp. 83–96.

Arconada-Alvarez, Santiago J., et al., 2017. The development and characterization of a novel yet simple 3D printed tool to facilitate phantom imaging of photoacoustic contrast agents. Photoacoustics 5, 17–24. https://doi.org/10.1016/j.pacs.2017.02.001.

ATOMMax® CIRS 711-H Specification sheet. Available at: http://www.cirsinc.com/wp-content/uploads/2020/07/711HN-DS-072220.pdfAccess, 24th of January.

Cerqueira, R.A.D., Maia, A.F., 2014. Development of thyroid anthropomorphic phantoms for use in nuclear medicine. Radiat. Phys. Chem. 95, 174–176. https://doi.org/10.1016/j.radphyschem.2012.12.038.

Daskalov, S., et al., 2019. Anthropomorphic physical breast phantom based on patient breast CT data: preliminary results. In: Mediterranean Conference on Medical and Biological Engineering and Computing. Springer, Cham, pp. 367–374. https://doi.org/10.1007/978-3-030-31635-8_44.

Diamantopoulos, S., et al., 2018. Theoretical and experimental determination of scaling factors in electron dosimetry for 3D-printed polylactic acid. Med. Phys. 45 (4), 1708–1714. https://doi.org/10.1002/mp.12790.

Esposito, G., et al., 2019. Investigation of the refractive index decrement of 3D printing materials for manufacturing breast phantoms for phase contrast imaging. Phys. Med. Biol. 64 (7), 075008 https://doi.org/10.1088/1361-6560/ab0670.

Feradov, Firgan, Marinov, Stoyko, Bliznakova, Kristina, 2019. Physical breast phantom dedicated for mammography studies. In: Mediterranean Conference on Medical and Biological Engineering and Computing. Springer, Cham, pp. 344–352. https://doi.org/10.1007/978-3-030-31635-8_41.

Filippou, V., Tsoumpas, C., 2018. Recent advances on the development of phantoms using 3D printing for imaging with CT, MRI, PET, SPECT, and ultrasound. Med. Phys. 45 (9), e740–e760. https://doi.org/10.1002/mp.13058.

Goldstone, K.E., 1989. Tissue substitutes in radiation dosimetry and measurement. In: ICRU Report 44. International Commission on Radiation Units and Measurements, USA, 1990.

Hamedani, B.A., et al., 2018. Three-dimensional printing CT-derived objects with controllable radiopacity. J. Appl. Clin. Med. Phys. 19 (2), 317–328. https://doi.org/10.1002/acm2.12278.

International Atomic Energy Agency, 2007. Dosimetry in Diagnostic Radiology: an International Code of Practice. IAEA, Vienna (Technical Report Series No. 457).

Koetzier, L.R., Mastrodicasa, D., Szczykutowicz, T.P., van der Werf, N.R., Wang, A.S., Sandfort, V., van der Molen, A.J., Fleischmann, D., Willemink, M.J., 2023. Deep learning image reconstruction for CT: technical principles and clinical prospects. Radiology 306 (3), e221257. https://doi.org/10.1148/radiol.221257.

Ogden, K.M., Morabito, K.E., Depew, P.K., 2019. 3D printed testing aids for radiographic quality control. J. Appl. Clin. Med. Phys. 20 (5), 127–134. https://doi.org/10.1002/acm2.12574.

Pereira, D.D., Cardoso, S.C., da Rosa, L.A.R., de Souza, F.M.L., de Sousa, J.V.M., Batista, D.V.S., et al., 2021. Validation of polylactic acid polymer as soft tissue substitutive in radiotherapy. Radiat. Phys. Chem. 189, 109726 https://doi.org/10.1016/j.radphyschem.2021.109726.

Pereira, D.D., Cardoso, S.C., Batista, D.V.S., de Souza, F.M.L., de Sousa, J.V.M., Gonçalves, O.D., da Rosa, L.A.R., 2022. Development of an anthropomorphic phantom based on 3D printing for assessment of dose delivered to the eye and adjacent tissues. Radiat. Phys. Chem. 199, 110292 https://doi.org/10.1016/j.radphyschem.2022.110292.

Savi, M., Andrade, M.A.B., Potiens, M.P.A., 2020. Commercial filament testing for use in 3D printed phantoms. Radiat. Phys. Chem. 174, 108906 https://doi.org/10.1016/j.radphyschem.2020.108906.

Savi, M., Villani, D., Andrade, M.A.B., Rodrigues Jr., O., Potiens, M.P.A., 2021. Study on attenuation of 3D printing commercial filaments on standard x-ray beams for dosimetry and tissue equivalence. Radiat. Phys. Chem. 182, 109365 https://doi.org/10.1016/j.radphyschem.2021.109365.

Savi, Matheus, Andrade, Marco Antônio Bertoncini, Villani, Daniel, Rodrigues Jr., Orlando, Maria da Penha Albuquerque Potiens, 2022. Development of radiopaque FFF filaments for bone and teeth representation in 3D printed radiological objects. Brazilian Journal of Radiation Sciences 10 (1). https://doi.org/10.15392/bjrs.v10i1.1739.

Villani, D., Rodrigues Jr., O., Campos, L.L., 2020. Dosimetric characterization of 3D printed phantoms at different infill percentages for diagnostic X-ray energy range. Radiat. Phys. Chem. 172, 108728 https://doi.org/10.1016/j.radphyschem.2020.108728.

Wang, Kan, et al., 2017. A review on the 3D printing of functional structures for medical phantoms and regenerated tissue and organ applications. Engineering 3 (5), 653–662. https://doi.org/10.1016/J.ENG.2017.05.013.